IEEE Access
Multidisciplinary | Rapid Review | Open Access Journal

Received October 24, 2020, accepted November 4, 2020, date of publication November 9, 2020, date of current version November 19, 2020.

Digital Object Identifier 10.1109/ACCESS.2020.3036883

Blind Detection of Underwater Acoustic Communication Signals Based on Deep Learning

YONGBIN LI, BIN WANG, GAOPING SHAO, SHUAI SHAO, AND XILONG PEI
PLA Strategic Support Force, Information Engineering University, Zhengzhou 450001, China
Corresponding author: Bin Wang (commutech@163.com)

ABSTRACT Blind detection of underwater acoustic communication (UWAC) signals is challenging in non-cooperative reception scenarios. Difficulties include but not limited to complex underwater acoustic channels, diversity of signal categories, and data scarcity. To address these problems, we propose a novel blind detection method for UWAC signals based on deep learning (DL). First, an impulsive noise preprocessor and a signal denoising generative adversarial network are built to mitigate the noise in the received signals. Second, a convolutional neural network-based binary classification network is built to automatically extract features and distinguish between the UWAC signals and noise. Moreover, a transfer data model is presented to overcome the insufficient data issue in the target water regions. The results of simulation experiments and practical signal tests both demonstrate that the proposed method is robust to ambient noise with wide dynamic ranges and complex distributions. Our approach significantly outperforms conventional algorithms and existing DL-based algorithms at low signal-to-noise ratios, while requiring no prior information about the testing channel.

INDEX TERMS Underwater acoustic communication signals, blind detection, generative adversarial network, convolutional neural network, noise reduction, transfer learning.

I. INTRODUCTION

Blind detection of underwater acoustic communication (UWAC) signals involves determining whether an observed underwater acoustic signal is a communication signal or ambient noise without any prior information. This task plays an important role in the modulation classification and information recovery of UWAC signals in non-cooperative reception scenarios.

Existing research on the blind detection of underwater acoustic signals has mainly been conducted on ship-radiated noise, via detecting their single-frequency linear spectrum [1]–[4]. However, the spectrums of different UWAC signals vary significantly with complex structural characteristics. Therefore, better detection techniques are required for UWAC signals. Although the likelihood ratio-based method [5] is not limited to the signal type, the construction of the likelihood function requires accurate knowledge of the noise distribution. Previous studies have developed a soft limiter detector (SLD) [6], a myriad detector [7], and a fractional lower-order moment detector (FLOMD) [8] for impulsive noise environments, but their performance depends on some prior information regarding the noise, such as the characteristic exponent and dispersion. Luo *et al.* [9] proposed a fractile-piecewise processing-based algorithm to estimate the above noise parameters and achieved better results. However, the estimation relied on the assumption that a pure noise segment is known in advance. The detection threshold also needed to be adjusted with the varying noise characteristics. Hence, due to the lack of prior information under complex marine environments, the aforementioned methods are inapplicable to non-cooperative UWAC signals. Furthermore, some approaches have been proposed for a particular type of signal, such as direct sequence spread spectrum (DSSS) [10], [11] by finding its distinct features. However, there are multiple UWAC signals with different features. This increases the complexity of the feature-based approach for large signal sets.

The associate editor coordinating the review of this manuscript and approving it for publication was Chengpeng Hao.

Considering the similarities between UWAC and radio communication (RC) signals, some blind detection methods for RC signals could serve useful. Blind detection algorithms for RC signals have been developed in the past decades and can be divided into two categories: conventional statistical detection theory (SDT)-based [12]–[15] and deep learning (DL)-based [16]–[19]. SDT-based methods require first designing the test statistics and then choosing appropriate thresholds or applying the support vector machines for judgement. This process relies on both the domain knowledge and prior information regarding the noise. Moreover, this approach is unstable for detection under marine noise characterized by wide dynamic ranges and complex distributions. In comparison, the recently developed DL-based methods have the advantage of automatic feature extraction. They not only require less domain and prior knowledge, but also show better robustness under noise of varying intensity. Therefore, the DL techniques seem to be more promising to resolve the existing problems going forward.

However, there are differences between UWAC and RC signals: (1) Marine ambient noise has a wider dynamic range and a more complex distribution. In particular, in shallow seas, noise usually exhibits the characteristic of impulse with varying intensity; (2) The multi-path effect of underwater acoustic channels is detrimental with long delay spreading, leading to significant distortion in the received signal; (3) UWAC signals are always transmitted in bursts, and the duration of a single burst might be short. Thus, it is difficult to acquire sufficient training data with a distribution that is similar to that of the testing data, to train a reliable network. These characteristics of UWAC signals pose new challenges to existing DL-based methods. Therefore, an effective weak-signal detection network should be designed, that can work robustly for a large signal set given the complex ambient noise and scarce training data.

In this paper, we propose a novel blind detection method for UWAC signals based on DL. The detection problem is redefined as a binary classification problem between UWAC signals and noise. First, an impulsive noise preprocessor (INP) and a signal denoising generative adversarial network (SDGAN) are built to mitigate the ambient noise in the received signal. Thereafter, the temporal waveforms of the denoised signals are fed to another convolutional neural network (CNN)-based binary classification network for automatic feature extraction and recognition. Furthermore, we adopt the idea of transfer learning and build a transfer data model. Based on this model, a transferred training set is generated to train a more stable detection network. The results of simulation experiments and practical signal tests both demonstrate the excellent performance of the proposed method. The detector trained on the transferred training set can effectively detect most common UWAC signals, including multiple frequency shift keying (MFSK), multiple phase shift keying (MPSK), orthogonal frequency division multiplexing (OFDM), linear frequency modulation (LFM) and DSSS under unknown channels.

This paper introduces an innovative approach for the blind detection of UWAC signals. The advantages and contributions of our work are summarized as follows:

- Most current methods require prior knowledge of the noise distributions and cannot adapt to time-varying noise environments. However, the proposed method does not have this dependency and is more robust to a large signal set under marine noise with wide dynamic ranges and complex distributions.
- The proposed INP and SDGAN exhibit good noise reduction capability, thus significantly enhancing the detection performance for weak signals; In comparison, the performance of existing methods decreases at low signal-to-noise ratios (SNRs).
- The proposed method is trained on a transferred training set, which requires no prior information about the testing channel, whereas existing DL-based methods require large amounts of data obtained from the testing channel environment.

The remainder of this paper is organized as follows: Section II introduces the proposed method and details of the algorithm. Section III presents the experimental results and discussion. Finally, Section IV concludes this paper.

II. SYSTEM MODEL AND PROPOSED METHOD

A. SIGNAL MODEL

The received signal can be modeled as follows:

$$y(t) = s(t) \otimes h(t) + w(t), \tag{1}$$

where, $s(t)$ represents the transmitted signals, including 2FSK, 4FSK, 8FSK, BPSK, QPSK, 8PSK, OFDM, LFM, and DSSS; $h(t)$ is the impulse response of the underwater acoustic channel, $w(t)$ is the ambient noise, and $\otimes$ represents the convolution operator. To better characterize the complexity of an actual marine environment, $w(t)$ is modeled as alpha-stable distributed noise.

For an MFSK signal [20], $s(t)$ can be expressed as follows:

$$s(t)_{\mathrm{MFSK}} = Ae^{j\theta}e^{j2\pi f_c t}\sum_{l=-\infty}^{\infty} e^{j2\pi f_\Delta (s_l t - lT_0)} g_c\left(t - lT_0\right), \tag{2}$$

where, $A, \theta, f_c, f_\Delta, T_0, M$ and $g_c(t)$ are the modulation amplitude, initial phase, carrier frequency, frequency deviation, symbol period, modulation order, and rectangular pulse-shaping filter, respectively, and $s_l \in \{\tilde{s}_m | \tilde{s}_m = 2m - 1 - M, m = 1, \cdots, M\}$ is the symbol transmitted within the lth period. The data symbols $\{s_l\}$ are assumed to be zero-mean independent and identically distributed (i.i.d.) random variables.

For an MPSK signal [21], $s(t)$ is expressed as follows:

$$s(t)_{\mathrm{MPSK}} = Ae^{j\theta}e^{j2\pi f_c t}\sum_{l=-\infty}^{\infty} b_l g_r\left(t - lT_0\right), \tag{3}$$

where, b_l, which is the lth transmitted symbol, can be represented as $\cos(\frac{2\pi(m-1)}{M})\,(m = 1, \cdots, M)$, and $g_r(t)$ is the

root-raised-cosine pulse-shaping filter. The data symbols $\{b_l\}$ are also i.i.d. random variables.

For an OFDM signal [21], the multiple subcarriers are modulated with BPSK; therefore, $s(t)$ can be expressed as follows:

$$s(t)_{\mathrm{OFDM}} = Ae^{j\theta}e^{j2\pi f_c t}\sum_{k=0}^{K-1}\sum_{l=-\infty}^{+\infty} a_{k,l}e^{j2\pi k\Delta f_k(t-lT_b)} \times g_r\left(t-lT_b\right), \quad (4)$$

where, K is the number of subcarriers, Δf_K is the frequency interval between two adjacent subcarriers, $g_r(t)$ is the root-raised-cosine pulse-shaping filter, T_b denotes the OFDM symbol period, $a_{k,l}$ denotes the lth transmitted symbol on the kth subcarrier, and the data symbols $\left\{a_{k,l}\right\}$ are also i.i.d. random variables.

For an LFM signal [22], $s(t)$ is expressed as follows:

$$s(t)_{\mathrm{LFM}} = Ae^{j\theta}e^{(j\pi k_0 t^2 + j2\pi f_0 t)}, \quad (5)$$

where k_0 is the chirp rate, and f_0 is the initial frequency.

For a DSSS signal [23], taking the BPSK modulation as an example, we can express $s(t)$ as:

$$s(t)_{\mathrm{DSSS}} = Ae^{j\theta}e^{j2\pi f_c t}\sum_{l=-\infty}^{\infty} d_l g_r\left(t-lT_c\right), \quad (6)$$

where T_c is the chip duration, $g_r(t)$ is the root-raised-cosine pulse-shaping filter, and d_l is the lth value of the sequence $d(t)$ after the spreading processing: $d(t) = r(t)c(t)$. $r(t)$ and $c(t)$ can be represented as $r(t) = \sum_{k=-\infty}^{\infty} r_k g_c\left(t-kT_a\right)$ and $c(t) = \sum_{k=0}^{N-1} p_k g_c\left(t-kT_c\right)$ respectively, where $r_k \in \{+1,-1\}$ is the kth transmitted symbol with the period T_a; $\{p_k, k=0,\ldots,N-1\}$ is the binary uncorrelated pseudo-noise (PN) sequence (± 1), and is short code; $g_c(t)$ and $g_r(t)$ are the rectangular and root-raised-cosine pulse-shaping filters, respectively.

The underwater acoustic channel is believed to be one of the most challenging channels due to the multi-path arrivals and complex ambient noise. Especially in shallow-water regions, industrial activities and shipping are frequently observed, not to mention the variety of marine life. These factors lead to the short, high-amplitude impulsive noise bursts [24], [25]. In [25], [26], the probability density functions (PDFs) of ambient noise from different shallow-water regions were collected and analyzed. The results indicate that this type of noise distribution is closer to an alpha-stable distribution and is much sharper than a Gaussian distribution. Further studies showed that the alpha-stable distribution, which is a unique distribution satisfying the generalized central limit theorem, can effectively characterize such heavy-tail distributed impulsive noise.

The characteristic function of an alpha-stable distribution can be expressed as [27]:

$$\phi(u) = \exp\left(jau - \gamma|u|^{\alpha}\left[1+j\beta\mathrm{sgn}(u)\omega(u,\alpha)\right]\right), \quad (7)$$

where,

$$\omega(u,\alpha) = \begin{cases}\tan(\pi\alpha/2) & \alpha \neq 1\\ (2/\pi)\log|u| & \alpha = 1,\end{cases} \quad (8)$$

$$\mathrm{sgn}(u) = \begin{cases}1 & u>0\\ 0 & u=0\\ -1 & u<0,\end{cases} \quad (9)$$

and $0 < \alpha \leq 2, -\infty < a < \infty, \gamma > 0$ and $-1 \leq \beta \leq 1$. The characteristic exponent α measures the intensity of the impulse; the lower the value of α, the higher the intensity. The special case $\alpha = 2$ corresponds to a Gaussian distribution. The location parameter a determines the center axis of the PDF. The dispersion γ is a measure of the distribution deviation around its mean value. The symmetry parameter β is used to describe the skewness of the PDF, and when $\beta = 0$, we have a symmetric alpha-stable ($S\alpha S$) distribution. When $a = 0$ and $\gamma = 1$, $S\alpha S$ becomes a standard alpha-stable distribution. Fig. 1 shows the examples of the standard alpha-stable distributed noise with different α values.

Moreover, because there is no second-order or higher-order statistics in a $S\alpha S$ distribution, the mixed signal-to-noise ratio (MSNR) is used to measure the power relationship between the signal and noise. The MSNR can be expressed as:

$$\mathrm{MSNR} = \left[10\lg\left(\sigma_s^2/\gamma\right)\right]\ (\mathrm{dB}), \quad (10)$$

where, σ_s^2 denotes the variance of the signal.

B. SIGNAL DETECTION MODEL

A blind detection model for UWAC signals is proposed, as shown in Fig. 2. First, to avoid the unfavorable effect of complex ambient noise, we adopt a noise reduction preprocessing method. Second, automatic detection is conducted on the denoised signal waveforms. Moreover, to resolve the problem of sparse data in different water regions and communication scenarios, we introduce the idea of transfer learning. Finally, a simulated transferred training set is generated for training a more reliable detection network.

As shown in Fig. 2, the detection model consists of offline training and online testing. Offline training includes the INP, SDGAN (composed of a generator (G) and discriminator (D)), and classifier (C). First, the INP is applied to suppress the high-amplitude impulsive noise in the received signal x_r, and x_p is obtained after normalization. Second, the SDGAN learns the distribution of the transmitted signal x_s through an adversarial training between G and D. The trained G can eliminate the low-amplitude noise that remains in x_p. Finally, the denoised signal $G(x_p, x_z)$ is fed to C for automatic feature extraction and binary classification. After offline training, online testing is implemented on the basis of the trained model. First, the INP and trained G are applied to preprocess the noisy testing signals. Subsequently, the trained C detects whether a UWAC signal exists.

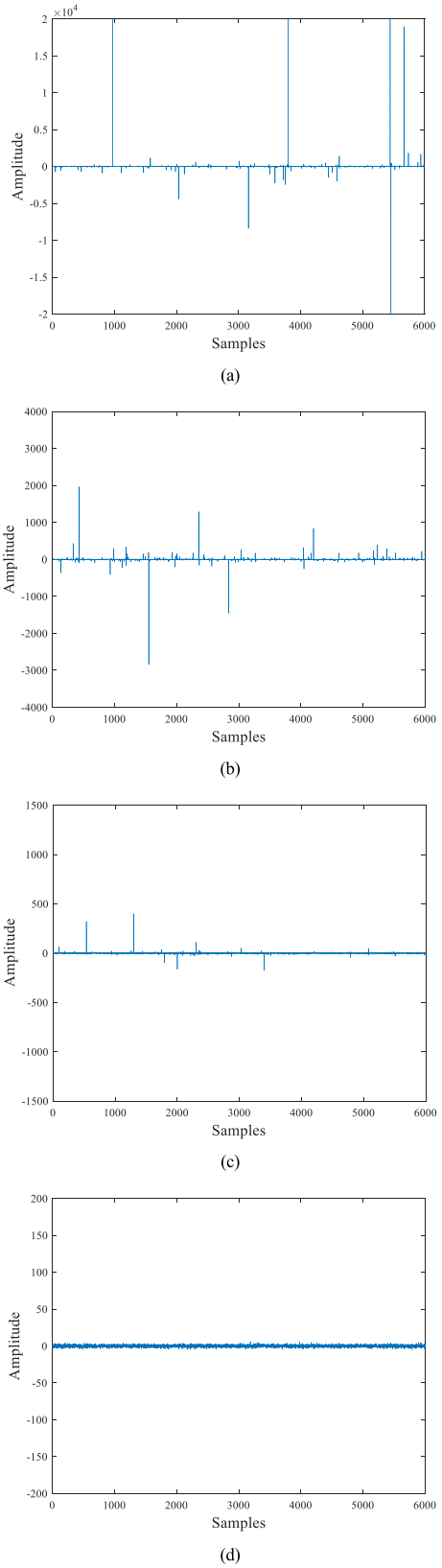

FIGURE 1. Temporal waveforms of standard alpha-stable distributed noise with different α values: (a) $\alpha = 0.8$; (b) $\alpha = 1.0$; (c) $\alpha = 1.5$; (d) $\alpha = 2.0$.

Marine ambient noise has a wide dynamic range in different underwater acoustic channels. From (1), (7), and Fig. 1, it is evident that the impulse intensity and noise power vary significantly with α and γ. In fact, the amplitude of impulse can be several orders of magnitude greater than those of the desired signals and the non-impulse components of the noise given the small value of α. The significant numerical differences among different waveform samples increase the probabilities of gradient imbalance and model non-convergence during the training of the SDGAN. Thus, it will be more difficult for the SDGAN to learn a good noise-reduction ability. To this end, it is necessary to adopt impulse mitigation and normalization preprocessing.

Common impulsive noise mitigation methods can be mainly divided into two categories: nonlinear transformation-based and threshold-based. In the former, a nonlinear transformation of the entire signal waveform is performed, such as logarithm transformation, Sigmoid transformation or arc tangent transformation [28]. Although the impulse can be effectively mitigated after the transformation, the desired signal is significantly affected. Hence, the nonlinear transformation-based methods are inapplicable for preparing the input to neural networks. In comparison, threshold-based methods (e.g., clipping and blanking) only process impulse locations with a high amplitude, with relatively less damage to the desired signal. The INP method adopted in this study can be considered a compromise between clipping and blanking and is proven to exhibit a better performance [29]. The objective of the INP is to nonlinearly suppress the regions where the amplitude is higher than the selected threshold τ_r in the received signal $x_r(t)$. The output of the INP can be represented as [29]:

$$x_{non}(t) = \begin{cases} x_r(t), & |x_r(t)| \le \tau_r \\ x_r(t)\left(\dfrac{\tau_r}{|x_r(t)|}\right)^2, & |x_r(t)| > \tau_r, \end{cases} \tag{11}$$

$$\tau_r = (1 + 2\tau_0)\tau_Q, \tag{12}$$

where, τ_0 is a constant coefficient (e.g., $\tau_0 = 1.5$ is considered in this work), and τ_Q is the second quartile of the absolute value of the received signal. Thereafter, $x_{non}(t)$ is further normalized to obtain the final output of the INP (i.e., the input to the SDGAN):

$$x_p(t) = \frac{x_{non}(t)}{\max(|x_{non}(t)|)}. \tag{13}$$

After the preprocessing by the INP, the high-amplitude impulsive noise is significantly suppressed; however, the remaining noise continues to affect the detection result. Conventional signal processing-based approaches first decompose the received signals, then find the components belonging to noise, and finally eliminate them. Unfortunately, domain knowledge is always required to help identify the noise components. The DL-based methods, which are a hotspot in the areas of image denoising and speech

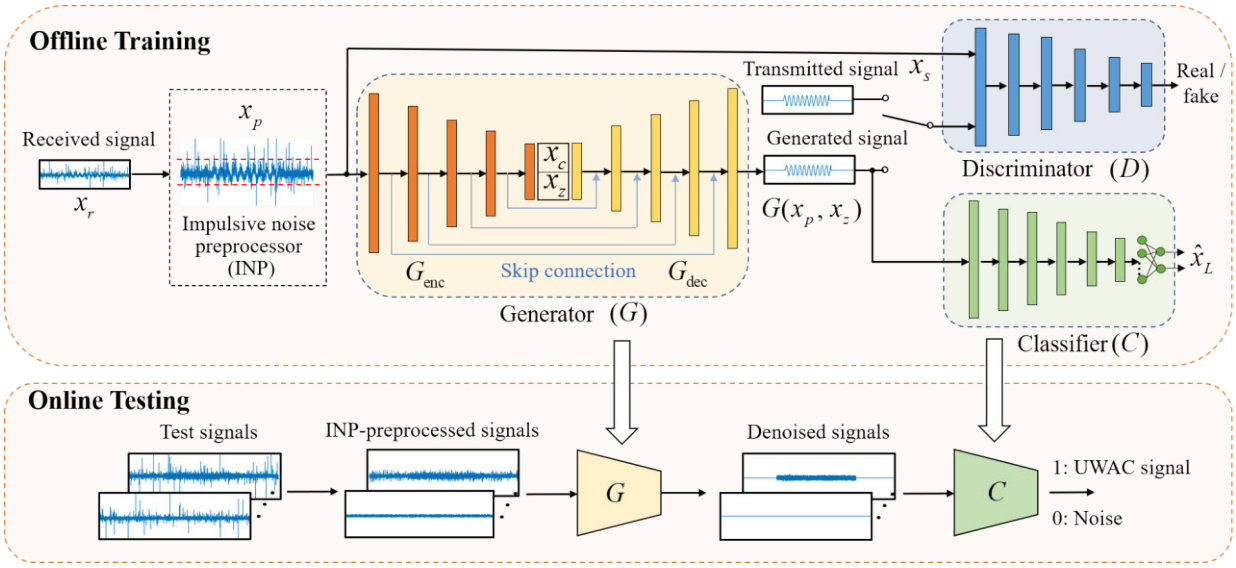

FIGURE 2. Proposed blind detection model for UWAC signals.

enhancement, can reduce this dependency [30]–[32]. In early DL-based methods, the denoising performance was measured by artificial quantized error metrics (such as the mean square error), which have certain limitations during training. This remained the case until the application of the generative adversarial network (GAN) [33]. The discriminator of the GAN can evaluate the quality of the generated data automatically using the learned metric. The new metric offers a better updating direction for the network, thus significantly improving the denoising performance.

The proposed SDGAN is derived from the standard generative adversarial network (SGAN), which is composed of a generative model and a discriminative model (i.e., G and D). The main difference is that an additional condition of the target data is added to the inputs of G and D. Thus, the generated data are more targeted, and D can better judge the generated data on the basis of the condition as well. Both these features make the generated data more consistent with the target data distribution. Hence, if the transmitted signal x_s and its noisy version x_p are considered as the target data and the additional condition, the trained GAN can project the input noisy signals onto the distribution of the clean target signals. This shows how the proposed SDGAN is used for noise reduction. However, because of the complex marine ambient noise, it remains challenging to conduct effective noise reduction for DL-based methods. Therefore, the network structure is further optimized by taking some cues from the speech enhancement relativistic generative adversarial network [32]. Finally, a relativistic loss function (RLF) with L1-norm and gradient penalty (GP) regularization are adopted to train the SDGAN.

After the noise preprocessing, a CNN-based classifier C is built for automatic feature extraction and recognition between the UWAC signals and noise. Typically, a CNN has fewer parameters than other networks and has been widely used in various classification problems. With the characteristics of weight sharing and local receptive field, it has evident advantages for the extraction of local features. As shown in the online testing part (see Fig. 2), the proposed INP and SDGAN have excellent noise reduction performance. The noise in the received noisy signals can be effectively suppressed to approximately 0, while the desired signals are well retained. Owing to the significant improvement in the SNR, C can now more easily detect the denoised signals.

C. NETWORK STRUCTURE

Among the modules of the proposed detection model shown in Fig. 2, G, D, and C are built with deep neural networks. To learn the temporally close correlations of the input waveforms better, G is designed to be fully convolutional. It is structured similar to a denoising auto-encoder [34], comprising an encoder G_{enc} and a decoder G_{dec}. G_{enc} aims to compress the original high-dimensional input x_r. During the compression, the useless or redundant information of x_r is gradually discarded, while the essential features are saved and mapped to a low-dimensional thought vector x_c. x_c is then concatenated with a latent noise vector x_z of the same size and is used alongside to reconstruct a denoised output $G(x_p, x_z)$ by G_{dec}. x_z is utilized to help improve the robustness to different inputs. Moreover, skip connections [35] are applied to connect each of the layer pairs of G_{enc} and G_{dec}. This type of identity mapping can help propagate information directly from the encoding layers to the deep decoding layers, thus preventing the fine-grained features (e.g., the phase information) from being lost during the dimension reduction. Furthermore, the gradients of the loss function can flow deeper, with the probability of vanishing gradient largely reduced.

TABLE 1. Structures of different modules in the detection model.

Modules	Layer	Parameters	Activation function	Layer	Parameters	Activation function
G	Conv1	(64, 32, 4)	PReLU	T-Conv1	(512, 32, 4)	PReLU
	Conv2	(128, 32, 4)	PReLU	T-Conv2	(256, 32, 4)	PReLU
	Conv3	(256, 32, 4)	PReLU	T-Conv3	(128, 32, 4)	PReLU
	Conv4	(512, 32, 4)	PReLU	T-Conv4	(64, 32, 4)	PReLU
	Conv5	(1024, 32, 4)	PReLU	T-Conv5	(1, 32, 4)	None
D	Conv6	(64, 32, 4)	Leaky ReLU	Conv10	(1024, 32, 4)	Leaky ReLU
	Conv7	(128, 32, 4)	Leaky ReLU	Conv11	(1, 1, 1)	None
	Conv8	(256, 32, 4)	Leaky ReLU	FC1	(8, 1)	None
	Conv9	(512, 32, 4)	Leaky ReLU			
C	Conv12	(16, 32, 4)	Leaky ReLU	Conv16	(256, 32, 4)	Leaky ReLU
	Conv13	(32, 32, 4)	Leaky ReLU	Conv17	(1, 1, 1)	Leaky ReLU
	Conv14	(64, 32,4)	Leaky ReLU	FC2	(8, 2)	Softmax
	Conv15	(128, 32, 4)	Leaky ReLU			

Considering the bandwidth and sampling rate of UWAC signals, the input dimension of G is designed to be 8192. A previous study [36] indicated that the strided convolution and fractional-strided transposed convolution are more stable for training a GAN than general pooling structures. Thus, G mainly consists of five one-dimensional strided convolution layers (Conv1–Conv5) and five one-dimensional fractional-strided convolution layers (T-conv1–T-conv5) with a stride of 4. The parametric rectified linear unit (PReLU) function [37] is employed for the activation of each layer.

D is built on the basis of G_{enc}, but with a few differences. First, D has two input channels (one for the additional condition x_p and the other for the transmitted signal x_s or generated signal $G(x_p, x_z)$). Second, the output of the fifth convolution layer follows another one-kernel convolution layer and a fully connected (FC) layer with a single output. They are designed for the compression of feature channels and authenticity judgement, respectively. Third, the activation function is updated to a Leaky ReLU function [37] with a parameter value of 0.3.

When it comes to C, a similar encoding structure is adopted with six strided convolution layers for feature extraction. There is an additional FC layer and a Softmax classifier for binary classification between the UWAC signals and noise. Let x_L be the data labels after one-hot encoding, then the output probability vector of the predicted labels can be expressed as:

$$\hat{x}_L = \begin{bmatrix} P(L_P = 0|Cout) \\ P(L_P = 1|Cout) \end{bmatrix} = \frac{1}{\sum_{i=1}^{2} \exp(Cout_i)} \begin{bmatrix} \exp(Cout_1) \\ \exp(Cout_2) \end{bmatrix}, \tag{14}$$

where,

$$Cout = f_{CNN}(G(x_p, x_z)), \tag{15}$$

L_P denotes the predicted labels, $Cout$ denotes the input vector of Softmax, and f_{CNN} is a nonlinear function formed by the layers before Softmax in C.

Table 1 lists the primary layers and parameters of the above three modules. The three parameters of the convolution layers and the transposed convolution layers represent the number of convolution kernels, kernel length, and stride, respectively. The two parameters of the FC layer represent the numbers of input and output nodes.

D. TRANSFER DATA MODEL

The core of training the SDGAN and C is to find the mapping relationship from the sampled training data to the feature space. To ensure that this mapping relationship can still be realized on the testing data, the training data are typically expected to exhibit the same distribution as the testing data. However, it is always difficult to acquire accurate channel information in unknown water regions and in different communication scenes. Therefore, there are insufficient data from the target channel that can be used to train a reliable model. To this end, we adopt the idea of transfer learning and present a transfer data model, which can be expressed as follows:

$$\tilde{y}(t) = s(t) + \tilde{w}(t), \tag{16}$$

where, $\tilde{y}(t)$ denotes the received signal, $s(t)$ denotes the transmitted signal, and $\tilde{w}(t)$ is also modeled as an alpha-stable distribution, with a characteristic exponent $\tilde{\alpha}$.

Compared with (1), (16) simplifies the influence of the multi-path channel. Although the distributions of the two data models are different, $y(t)$ and $\tilde{y}(t)$ still have the same signal set, i.e., they contain the same components of the transmitted signals. Meanwhile, the output data distribution of G remains unchanged, which is an effective constraint on the input of C. Based on (16), we can simulate and generate signal examples with noise of different distributions and power. The model trained on such a data-rich training set is expected to be more robust to noise of wide dynamic ranges and complex distributions.

E. JOINT TRAINING OF SDGAN AND CLASSIFIER

Fig. 2 shows that the effective noise reduction and detection is mainly achieved via the joint training of SDGAN and C. For the SDGAN, the key to its adversarial training is to construct a suitable loss function that can better measure the distance between the target and generated data distributions. The SGAN adopts the binary cross entropy (BCE) [33] as its loss function, which essentially measures

the Jensen–Shannon divergence (JSD) of different distributions. However, because the training data are always sampled from the low-dimensional manifold of a high-dimensional space, cross items seldom exist between two distributions. This makes the JSD more likely to remain a high value (i.e., vanishing gradient) and difficult to optimize. Other problems include non-convergence [36] and mode collapse [38].

To resolve these issues, various improvements have been proposed, such as the least-squares function [39], Wasserstein distance [40], and GP [41]. A recent study [42] has shown that there is a significant drawback in the mechanism of the SGAN. The loss function of the SGAN helps increase the probability of fake data being real, whereas the probability of real data being real remains unchanged. This result contradicts the prior assumption in the theoretical derivation of the SDGAN, where half the data are real or fake in a training batch. For this assumption to hold, the RLF [42] is proposed for an improvement. The RLF estimates the probability of given real data being more realistic than randomly sampled fake data. This modification not only increases the probability of fake data being judged as real, but also reduces the probability of real data being real. Moreover, the RLF exhibits a better performance than the other aforementioned loss functions in the areas of image generation [42] and speech enhancement [32].

Therefore, the RLF is also utilized in this study to narrow the distribution distance between $G(x_p, x_z)$ and x_s. The RLF can be denoted by $L_{RS}(G)$ and $L_{RS}(D)$ for G and D, respectively. Moreover, an L1-norm term $L_{L_1}(G)$ of first order is added to help constrain the denoising error. Another GP term $L_{GP}(D)$ is also introduced in D to help stabilize the training and avoid exploding or vanishing gradients.

The total loss functions for G and D can be respectively expressed as:

$$\begin{aligned} L_G &= L_{RS}(G) + L_{L_1}(G) \\ &= -\mathrm{E}_{(x_s,x_p)\sim(Q_s,Q_p)}\left[\log(\sigma(D(G(x_p,x_z),x_p) - D(x_s,x_p)))\right] \\ &\quad + \lambda_{L1}\left\|G(x_p,x_z) - x_s\right\|_1, \end{aligned} \tag{17}$$

$$\begin{aligned} L_D &= L_{RS}(D) + L_{GP}(D) \\ &= -\mathrm{E}_{(x_s,x_p)\sim(Q_s,Q_p)}\left[\log(\sigma(D(x_s,x_p) - D(G(x_p,x_z),x_p)))\right] \\ &\quad + \lambda_{GP}\mathrm{E}_{\tilde{x},x_p\sim\tilde{Q}}\left[(\left\|\nabla_{\tilde{x},x_p}D(\tilde{x},x_p)\right\|_2 - 1)^2\right], \end{aligned} \tag{18}$$

where, σ is the Sigmoid function, Q_s and Q_p represent the probability distributions of x_s and x_p, respectively, $\tilde{Q}$ is the joint probability distribution of x_p and $\tilde{x}$, and $\tilde{x} = \mu x_s + (1-\mu)G(x_p, x_z)$, where μ is a random real number between 0 and 1.

For the classifier C, the BCE is adopted to calculate the distribution distance between the real category labels and the predicted labels

$$L_C = -\frac{1}{N}\sum_{j=1}^{N}\sum_{i=1}^{2} x_{Li}^{j}\log(\hat{x}_{Li}^{j}), \tag{19}$$

where, N denotes the mini-batch size.

The network training and prediction is conducted with the DL library, Pytorch, on a single NVIDIA TITAN RTX GPU. The model is optimized using the Adam algorithm [43], with a learning rate of 0.0001, and $N = 128$. The hyper-parameters λ_{L1} and λ_{GP} are set to 200 and 10, respectively, to reach the same order of magnitude as those of $L_{RS}(G)$ and $L_{RS}(D)$. The training is continued until all the parameters of the detector $\theta_{Detector}$ converge. The joint training algorithm is detailed in Table 2.

TABLE 2. Joint training algorithm of the SDGAN and classifier.

Require: Training dataset S, learning rate l_r, batch size N, loss function weights λ_{L1} and λ_{GP}.

1. Initialization

- All weights of different layers are initialized with the Kaiming uniform distribution [37], and biases initialized with zero.

2. Training:

While $\theta_{Detector}$ has not converged **do**

- Sample N signal examples $\left\{(x_s^1, x_r^1, x_L^1), \ldots, (x_s^N, x_r^N, x_L^N)\right\}$ from S and N noise examples $\left\{x_z^1, \ldots, x_z^N\right\}$ from standard normal distribution.
- Perform INP on $\left\{x_r^1, \ldots, x_r^N\right\}$ to obtain $\left\{x_p^1, \ldots, x_p^N\right\}$.
- Generate denoised signal examples $\left\{G(x_p^1, x_z^1), \ldots, G(x_p^N, x_z^N)\right\}$.
- Calculate the probability vectors of the predicted labels $\left\{\hat{x}_L^1, \ldots, \hat{x}_L^N\right\}$.
- Calculate the loss function of D L_D and update θ_D using the Adam optimizer by gradient descent with $\nabla_{\theta_d}\frac{1}{N}\sum_{i=1}^{N} L_D(x_s^i, x_p^i, x_z^i)$.
- Calculate the loss function of G L_G and update θ_G using the Adam optimizer by gradient descent with $\nabla_{\theta_G}\frac{1}{N}\sum_{i=1}^{N} L_G(x_s^i, x_p^i, x_z^i)$.
- Calculate the loss function of C L_C and update θ_C using the Adam optimizer by gradient descent with $\nabla_{\theta_C}\frac{1}{N}\sum_{i=1}^{N} L_C(x_L^i, \hat{x}_L^i)$.

end while

III. NUMERICAL RESULTS AND DISCUSSION

A. SIGNAL PARAMETERS AND DATASET

All the signals are generated on the basis of the signal model described in Section II.A, with a sampling rate of 48 kHz. The center frequency of the LFM signals and the carrier frequencies of the other signals randomly vary in the range of 15 to 16 kHz. For the DSSS signal, the m-sequence is adopted as the PN sequence.

Table 3 lists the detailed signal parameters, where, / implies that the parameter is not involved for the corresponding

TABLE 3. Signal parameters.

Signal types	Symbol rate (Baud)	Modulation index	Roll-off factor	Cyclic prefix	No. Subcarriers	Chirp rate (Hz/ms)	m-sequence period
2FSK	[530, 1k]	1	/	/	/	/	/
4FSK	[320, 600]	1	/	/	/	/	/
8FSK	[170, 330]	1	/	/	/	/	/
OFDM	{100, 120, 200}	/	0.25	0.25	16	/	/
MPSK	{1.6k, 2k, 2.4k, 3k}	/	0.25	/	/	/	/
DSSS	{1.6k, 2k, 2.4k, 3k}	/	0.25	/	/	/	63
LFM	/	/	/	/	/	[60, 100]	/

signal, and [ ] and { } imply that the parameter is randomly selected within a closed interval and the given items.

The offline training is implemented on the transferred training set, which is based on the transfer data model expressed in (16). $\tilde{\alpha}$ is randomly selected in the range of [1.5, 2], with MSNR in the range of $[-10, 10]$ dB.

UWAC signals are transmitted in bursts, with unknown start and end times. Therefore, to improve the practicability of the method in real-world reception scenarios without prior information, a training signal example structure is designed, as shown in Fig. 3. The processing data block is composed of a communication data segment and two pure noise data segments. The duration L and location of the communication data block are both random, and $0 \leq L \leq L_n$, where, L_n is the length of the processing data block (i.e., the input dimension of G, 8192). The above signal structure is applied to generate 2000 examples for each type of signal. Moreover, the same number of pure noise examples is generated as the sum of the UWAC signals. Thus, we build a transferred training set containing a total of 36000 examples to train the network. Different testing sets will be given in the specific experiments.

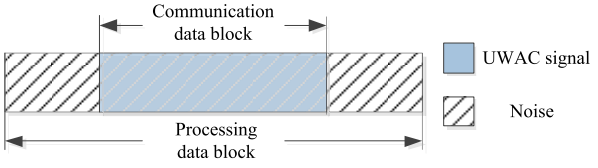

FIGURE 3. Structure of a training signal example.

B. SIMULATION EXPERIMENTS AND DISCUSSION

1) PERFORMANCE COMPARISON

To prove the effectiveness and superiority of the proposed method, we compared its performance with those of existing methods both under $S\alpha S$ noise ($\alpha < 2$) and Gaussian noise.

Based on (1), a typical underwater acoustic sparse channel, as reported in [44], is utilized to simulate the unknown channel $h(t)$, whose transfer function is as follows:

$$H(z) = 1 - 0.5z^{-14} + 0.4z^{-18}. \tag{20}$$

Because the detection threshold is not required for the presented method, the probability of false alarm (Pf) is independent of the MSNR and is only related to α under the $S\alpha S$ noise environment. First, we build two testing sets with $\alpha = 1.8$ and $\alpha = 1.5$. Each testing set contains 2000 noise examples, which are used to obtain the Pf values. The MSNR of the noisy UWAC testing signals varies from -15 to 5 dB with an interval of 2 dB. Another 1600 signal examples are generated for calculating the probability of detection (Pd) under different MSNRs. To clearly show the effectiveness of the INP and SDGAN, we select a BPSK example under the conditions of $\alpha = 1.5$, MSNR $= -1$ dB, and $L = 4096$. The temporal waveforms in different processing stages are compared in Fig. 4.

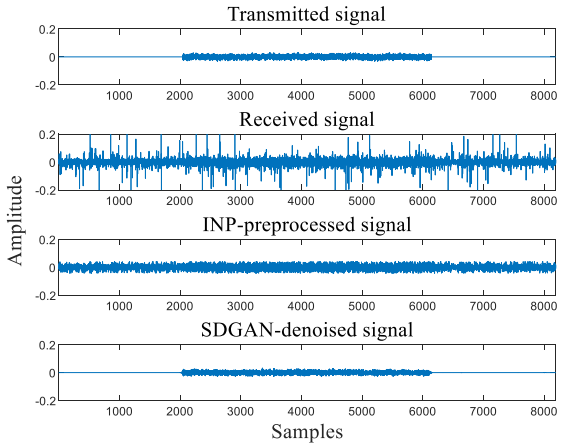

FIGURE 4. BPSK temporal waveforms in different processing stages, including the transmitted one, received one, INP-preprocessed one, and SDGAN-denoised one.

Fig. 4 shows that compared with the transmitted signal, the received signal is severely distorted due to the heavy $S\alpha S$ noise. After the preprocessing by the INP, the high-amplitude impulse is largely suppressed. The following SDGAN further reduces the remaining low-amplitude noise, and finally the start and end times of the originally transmitted signal are clearly visible.

To further perform the necessity of the INP in our method, Fig. 5 gives a comparison of the denoising performance of

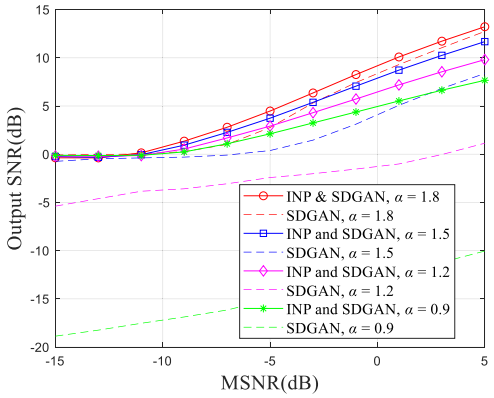

FIGURE 5. Denoising performance of the SDGAN and the combination of INP and SDGAN under different α values.

the SDGAN with that of the combination of the INP and SDGAN under the alpha-stable distributed noise. The output SNR is utilized to measure the denoising performance of the two methods, which can be expressed as [45]:

$$\text{Output SNR} = 10\lg\left(\frac{\sum_{l=1}^{L_n} s(l)^2}{\sum_{l=1}^{L_n} (s(l) - \hat{s}(l))^2}\right) \text{(dB)}, \qquad (21)$$

where, $s(l)$ and $\hat{s}(l)$ are the samples of a transmitted signal example and its denoised version, respectively.

As shown in Fig. 5, compared with a single SDGAN, incorporating the INP does help improve the denoising performance, and the lower the value of α, the greater the improvement. Thus, it can be concluded that the INP can effectively suppress the high-amplitude impulse and is required in our method to deal with complex marine ambient noise.

Furthermore, a detection performance comparison is made in Fig. 6 among the proposed method (i.e., INP + SDGAN + C), the proposed method without INP (i.e., SDGAN + C), the FLOMD [8], and the SLD [6] methods. The Pf values of the former two DL-based methods are fixed given a specific α, i.e., 0.65% and 1.0% when $\alpha = 1.8$; and 0.8% and 2.4% when $\alpha = 1.5$. By contrast, the Pf and Pd values of the latter two SDT-based methods vary with the given thresholds. For the sake of comparison, we select their detection performance when Pf = 1.0% from the receiver operating characteristic (ROC) curves. Moreover, some prior information about the impulsive noise intensity and power is used to obtain the ROCs under different MSNRs.

As shown in Fig. 6(a), the proposed method has the highest Pd value and the lowest Pf value when $\alpha = 1.8$. Pd reaches approximately 99% even at a low MSNR of -10 dB. However, the lack of INP results in a slight increase in the Pf value, and the Pd performance decreases by approximately 1 dB. Nevertheless, there is still a gain of 3 dB compared with the SLD approach, indicating that the SDGAN itself has the capability to adapt to weak impulsive noise.

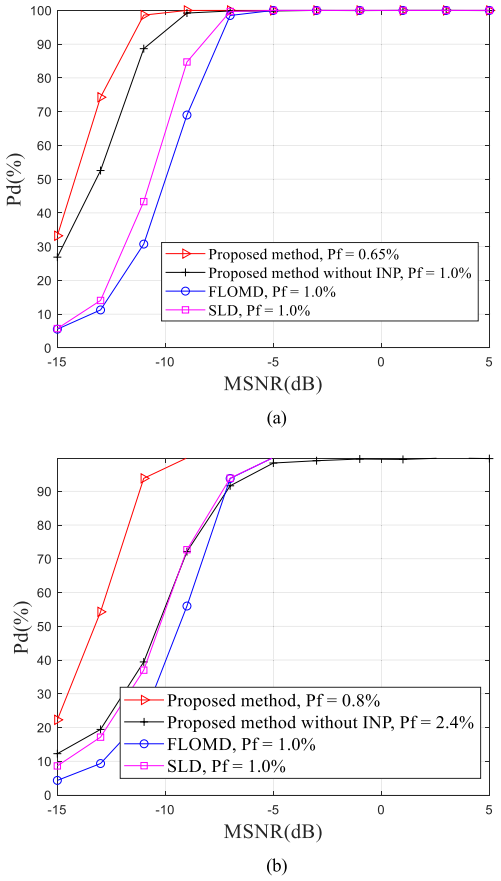

FIGURE 6. Detection performance of different methods under different α values: (a) $\alpha = 1.8$; (b) $\alpha = 1.5$.

When α decreases to 1.5, the intensity of the impulse is largely increased. As shown in Fig. 6(b), the performance of the proposed method without the INP dynamically degrades, with the Pf value reaching to 2.4%. The overall performance is even worse than that of the SLD method. Although the performance of the proposed method also slightly declines, it still has a gain of approximately 3 dB compared with that of the SLD method. These results demonstrate the effectiveness and excellent performance of our method under $S\alpha S$ noise, as well as the importance of the INP.

Finally, Table 4 presents a comparison of the performance of our method and two other DL-based methods under Gaussian noise. Our approach has a high Pd of 99.4% even when SNR $= -11$ dB, and a low Pf of 0.85%. Both the indexes are much better than those of existing DL-based methods. Therefore, we can conclude that the proposed method outperforms existing DL-based methods under Gaussian noise.

In our method, the received signals are first denoised by the INP and SDGAN, and are then used for detection. However, the detection process is directly performed on the received noisy signals in previous methods. Thus, the improved SNR may be an important factor leading to a better performance in our method. Moreover, the filter (kernel) length of the

TABLE 4. Pd and Pf of different methods under Gaussian noise.

Methods	−15 dB	−13 dB	−11 dB	−9 dB	7 dB	−5dB	−3 dB
Proposed method (Pf = 0.85%)	42.9%	83.7%	99.4%	100.0%	100.0%	100.0%	100.0%
Method in [17] (Pf = 5.0%)	13.0%	18.0%	28.0%	47.5%	71.0%	93.0%	99.5%
Method in [18] (Pf = 5.92%)	23.5%	39.0%	58.5%	84.5%	99.0%	99.5%	100.0%

convolutional layers in the proposed SDGAN and classifier (i.e., 32) is larger than those in existing DL-based methods [17], [18] (i.e., 10 and 20). Typically, a larger filter length means a better frequency response, so the convolutional layers in the proposed networks may extract better features for detection.

2) PERFORMANCE UNDER DIFFERENT CONDITIONS

In this section, several factors that may affect the detection performance of the proposed method are evaluated, including the MSNR range of the training data (TMSNR), underwater acoustic channels, intensity of impulsive noise (i.e., the value of α), and duration of the communication data block L.

Firstly, to obtain a relatively good performance in terms of Pd and Pf under different MSNRs, an appropriate TMSNR is required to train a reliable model. We construct four training sets with different TMSNRs, including [−15, 10] dB, [−10, 10] dB, [−5, 10] dB and [0, 10] dB. Moreover, we adopt the testing set with $\alpha = 1.5$, described in Section III.B, to obtain the Pd and Pf performance. Fig. 7 and Table 5 show the results.

As shown in Fig. 7 and Table 5, the model trained under high TMSNR has the lowest Pf, whereas the Pd performance is poor under low MSNR testing data. In the training process, the objective of the model is to distinguish between the high MSNR UWAC signals and noise. Because they have a considerable difference, the probability of the trained model to judge noise as UWAC signals is very low (i.e., low Pf). As the testing MSNR decreases, the noisy UWAC signals become increasingly similar to noise. The trained model is unfamiliar to these signals and is more likely to misjudge them as noise. Thus, the trained model is unable to correctly recognize low MSNR UWAC signals (i.e., low Pd).

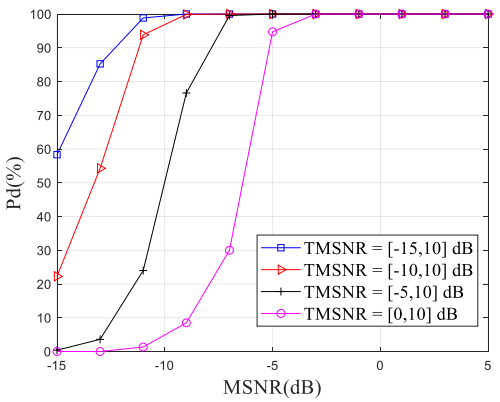

FIGURE 7. Detection performance under different TMSNRs.

TABLE 5. Pf under different TMSNRs.

[−15, 10] dB	[−10, 10] dB	[−5, 10] dB	[0, 10] dB
9.2%	0.8%	0.0%	0.0%

As the low bound of the TMSNR decreases, the trained model has a higher Pd on the low MSNR testing signals, as well as an increasing Pf on noise. In fact, when the TMSNR is low enough, the noisy signals and noise are too similar to distinguish. However, in the training process, the preset data labels and the optimizer will constantly require the model to give low MSNR signals a correct prediction. Thus, the probability of the trained model to correctly identify the low MSNR signals will improve (i.e., a higher Pd). Because of the similarity, the probability of noise being judged as UWAC signals will also increase (i.e., a higher Pf). When the low bound of the TMSNR decreases from −10 dB to −15 dB, Pd on low MSNR testing signals slightly increases, whereas Pf significantly increase from 0.8% to 9.2%. This indicates that the trained model has a poor performance in recognizing between those low MSNR signals and noise. Moreover, as shown in the curve of TMSNR = [−10, 10] dB, the detection performance of the trained model deteriorates sharply when the testing MSNR is lower than −10 dB. Therefore, under the experiment sets adopted in this study, the lower bound of the TMSNR should not be lower than −10 dB.

Secondly, to evaluate the impact of impulse intensity, we compared the detection performance under different α values. And a similar testing data format to the one described in Section III.B is adopted to obtain the Pd and Pf performance. Fig. 8 and Table 6 show the results.

TABLE 6. Pf under different impulse intensities.

$\alpha = 0.6$	$\alpha = 0.9$	$\alpha = 1.2$	$\alpha = 1.5$	$\alpha = 1.8$
0.55%	0.35%	0.85%	0.80%	0.65%

As shown in Fig. 8, Pd declines with the decrease in α. When α decreases from 1.8 to 0.9, Pd performance suffers a decline by approximately 3 dB. Nevertheless, the proposed method still has a Pd of approximately 75% at a low

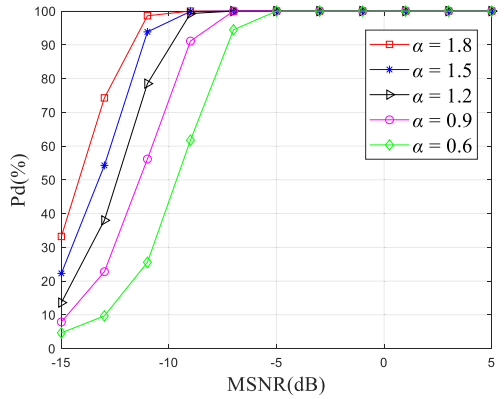

FIGURE 8. Detection performance under alpha-stable distributed noise with different α values.

MSNR of -10dB. However, when α continues to drop to 0.6, Pd declines sharply to 45% and is not applicable. In fact, the high-amplitude impulse decreases the detection performance by making it more difficult for the INP and SDGAN to perform noise reduction, as shown in Fig. 5. Moreover, Table. 6 shows that the Pf values fluctuate within the range of [0.35%, 0.85%] without any evident rising or falling trend with the change in α. This indicates that the proposed method is robust against false alarms.

Thirdly, to prove that the proposed detection method is robust against underwater acoustic channels, we compared the detection performance under different channels. The widely used Bellhop channel simulation software was adopted to generate five sparse underwater acoustic channels (h_A, h_B, h_C, h_D, and h_E) based on the famous Argo ocean database. Table 7 lists the detailed channel parameters. Different coordinates and transmission conditions were utilized to ensure the diversity of the channel characteristics.

TABLE 7. Parameters of different underwater acoustic channels.

Channels	Coordinates	Transmitter depth (m)	Distance (km)	Receiver depth (m)
h_A	(80.5°E, 30.5°S)	50	15	50
h_B	(170.5°E, 55.5°N)	100	8	100
h_C	(220.5°E, 0.5°N)	200	10	200
h_D	(99.5°W, 20.5°S)	50	5	200
h_E	(39.5°W, 30.5°N)	200	12	50

Their transfer functions are listed as follows:

$$H_A(z) = 0.07+0.2z^{-140} + z^{-653} + 0.23z^{-817} + 0.05z^{-876},$$
$$H_B(z) = 0.7 + 0.6134z^{-541} + 0.971z^{-945} + z^{-1261},$$
$$H_C(z) = 1 + 0.58z^{-3369} + 0.56z^{-3581},$$
$$H_D(z) = 0.49 + 0.18z^{-169} + z^{-311},$$
$$H_E(z) = 0.47 + 0.04z^{-575} + z^{-746} + 0.75z^{-3379} + 0.47z^{-4210}.$$

Because the sampling rate is set to 48 kHz, the maximum propagation delays of these channels vary from 6.5 to 87.7 ms. Furthermore, Fig. 9 shows the amplitude-frequency response curves of the different underwater acoustic channels.

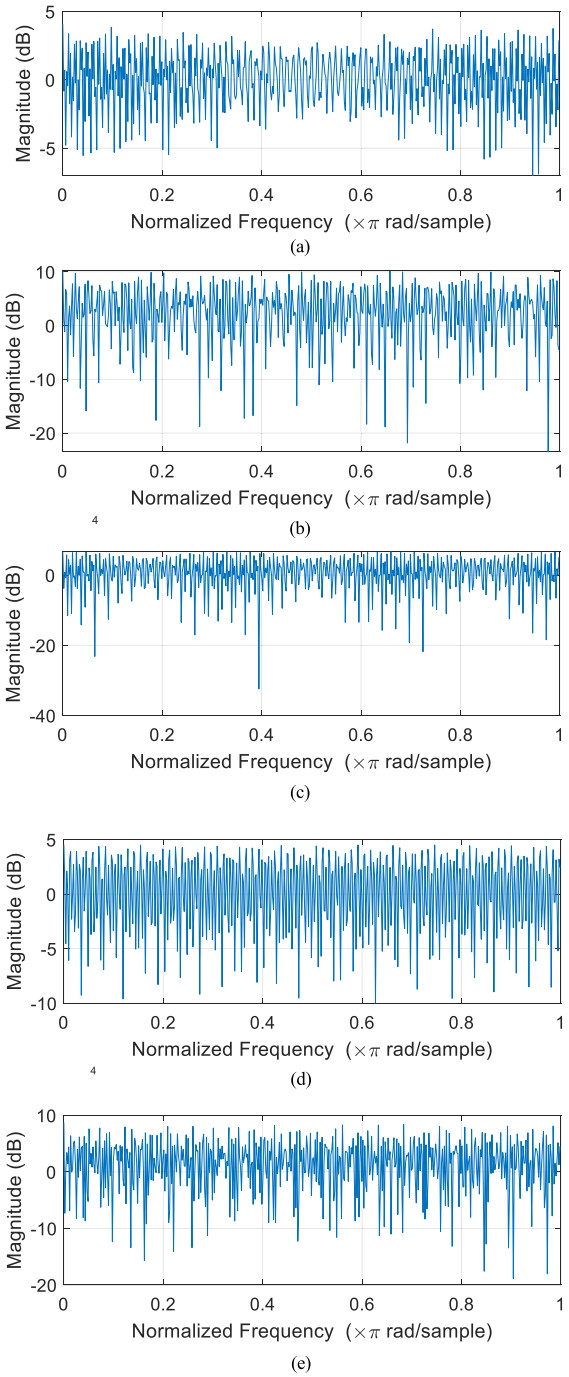

FIGURE 9. Amplitude-frequency response curves of the different underwater acoustic channels: (a) h_A; (b) h_B; (c) h_C; (d) h_D; (e) h_E.

As shown in Fig. 9, these channels have different frequency selective fading characteristics. The fading due to channels h_B, h_C, and h_E are deep at some frequencies, whereas that

of h_D is shallower. Moreover, the channel h_A has relatively the best frequency characteristics, and the decline is less than 5 dB overall. We further built five testing sets under each of these channels with $\alpha = 1.5$. Fig. 10 shows the detection performance under the different underwater acoustic channels.

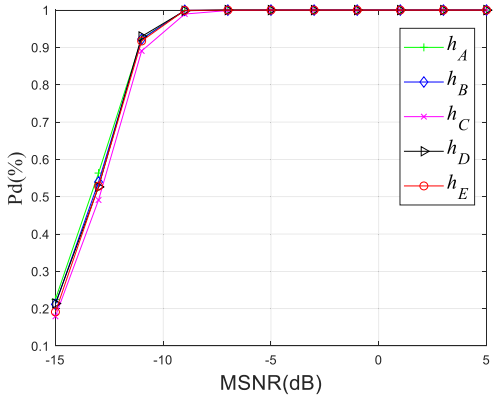

FIGURE 10. Detection performance under different underwater acoustic channels.

As shown in Fig. 10, there is little difference in the detection performance under the above five channels. This confirms the robustness of the proposed method to different underwater acoustic channels.

Eventually, given that the practical UWAC signals are transmitted in bursts with an uncertain duration, the detection performance under different burst durations is tested, including $L = 1024, L = 2048, L = 4096$, and $L = 8192$. The testing dataset is generated under $S\alpha S$ noise with $\alpha = 1.5$. Fig. 11 shows the results.

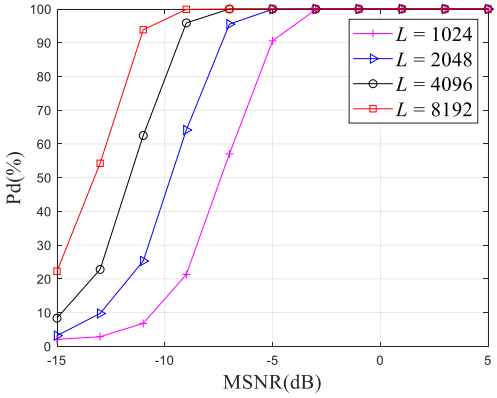

FIGURE 11. Detection performance under different burst durations.

As shown in Fig. 11, with the increase in L, the detection performance is gradually improved, though at a decreasing rate. When L increases from 1024, 2048, and 4096 to 2048, 4096, and 8192, respectively, the performance gains reach approximately 2.5, 2, and 1.5 dB. The improved performance can be attributed to the increased information available for detection.

C. PRACTICAL SIGNAL TESTS

In this section, the performance of our method is further tested on practical signals. On July 18, 2019, a sea trial was conducted in Wuyuan Bay, Xiamen. Fig. 12(a) shows the experimental setup, where S1 and S2 denote the transmitter and receiver locations, respectively, and the transmission distance is approximately 545 m. Moreover, the water depth in this water region varies from approximately 6 to 8 m. A transmitting node with an omnidirectional transducer and a receiving node with a single hydrophone were placed 3 m below the water surface. The utilized broadband hydrophone, as depicted in Fig. 12(c), is the RB9-ETH model (Ocean Sonics). Furthermore, a lake trial was conducted in an artificial lake on campus on April 27, 2020. Fig. 12(b) shows the experimental setup, where S3 and S4 denote the transmitter and receiver locations, respectively. The same experimental equipment was used. During the experiments, the sampling rate of the utilized hydrophone was set to 64 kHz, and the corresponding receiving frequency ranged from 10 Hz to 25.6 kHz. However, for trained networks, the testing data should to be in the same format as the training data, i.e., their sampling rates should match. Thus, the received signals were resampled before testing.

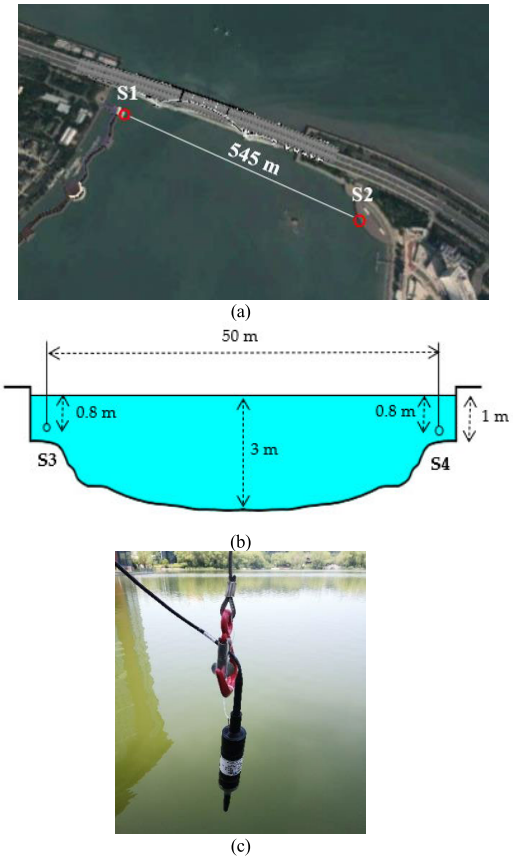

FIGURE 12. Experimental setup and equipment: (a) Experimental setup of the sea trial in Wuyuan Bay; (b) Experimental setup of the lake trial; (c) Utilized hydrophone.

In each experiment, 7000 low-SNR UWAC signal examples were collected by reducing the transmitting power.

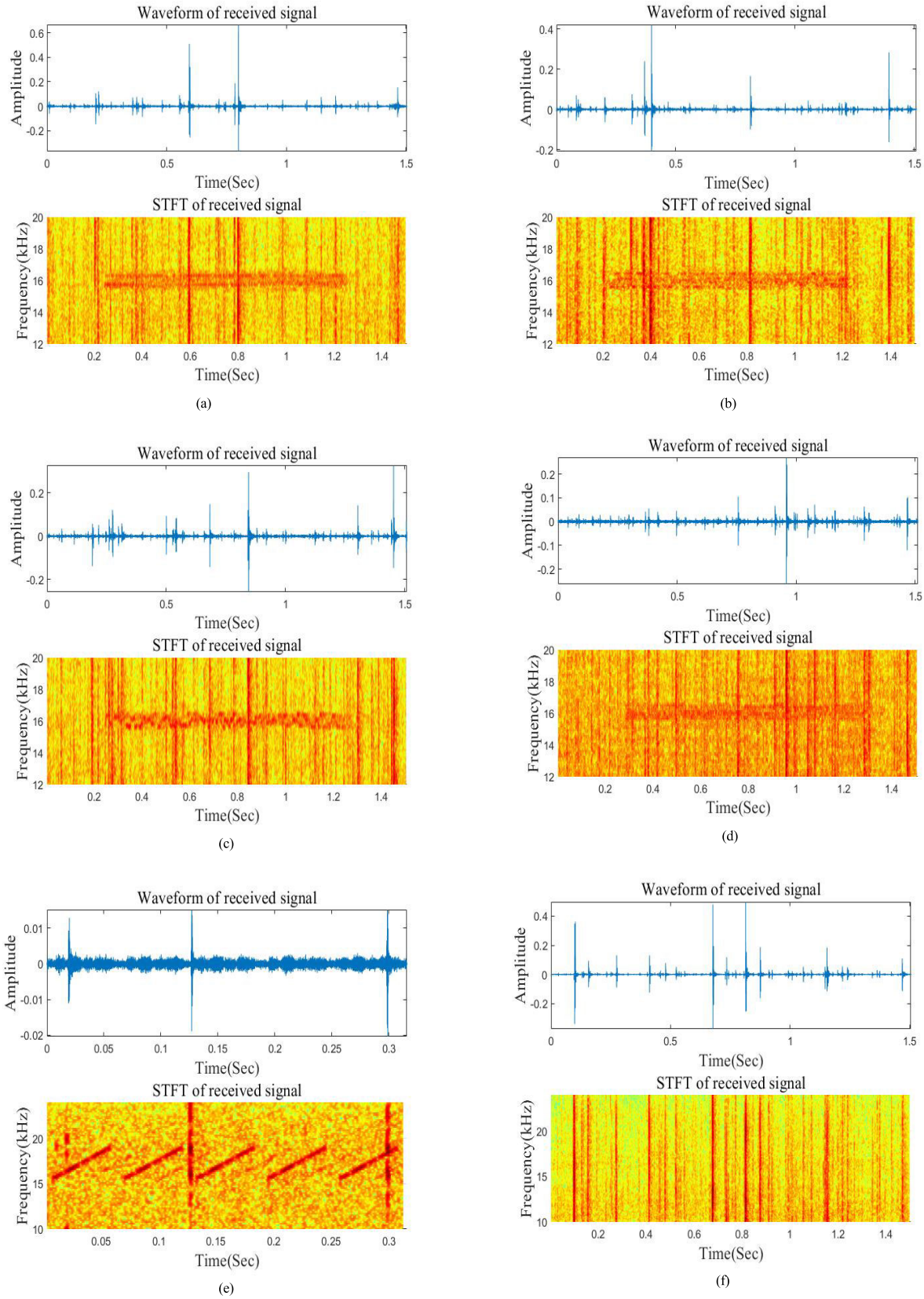

FIGURE 13. Temporal waveforms and STFT of different UWAC signals and noise examples collected from Wuyuan Bay: (a) 2FSK; (b) 4FSK; (c) 8FSK; (d) BPSK; (e) LFM; (f) Noise.

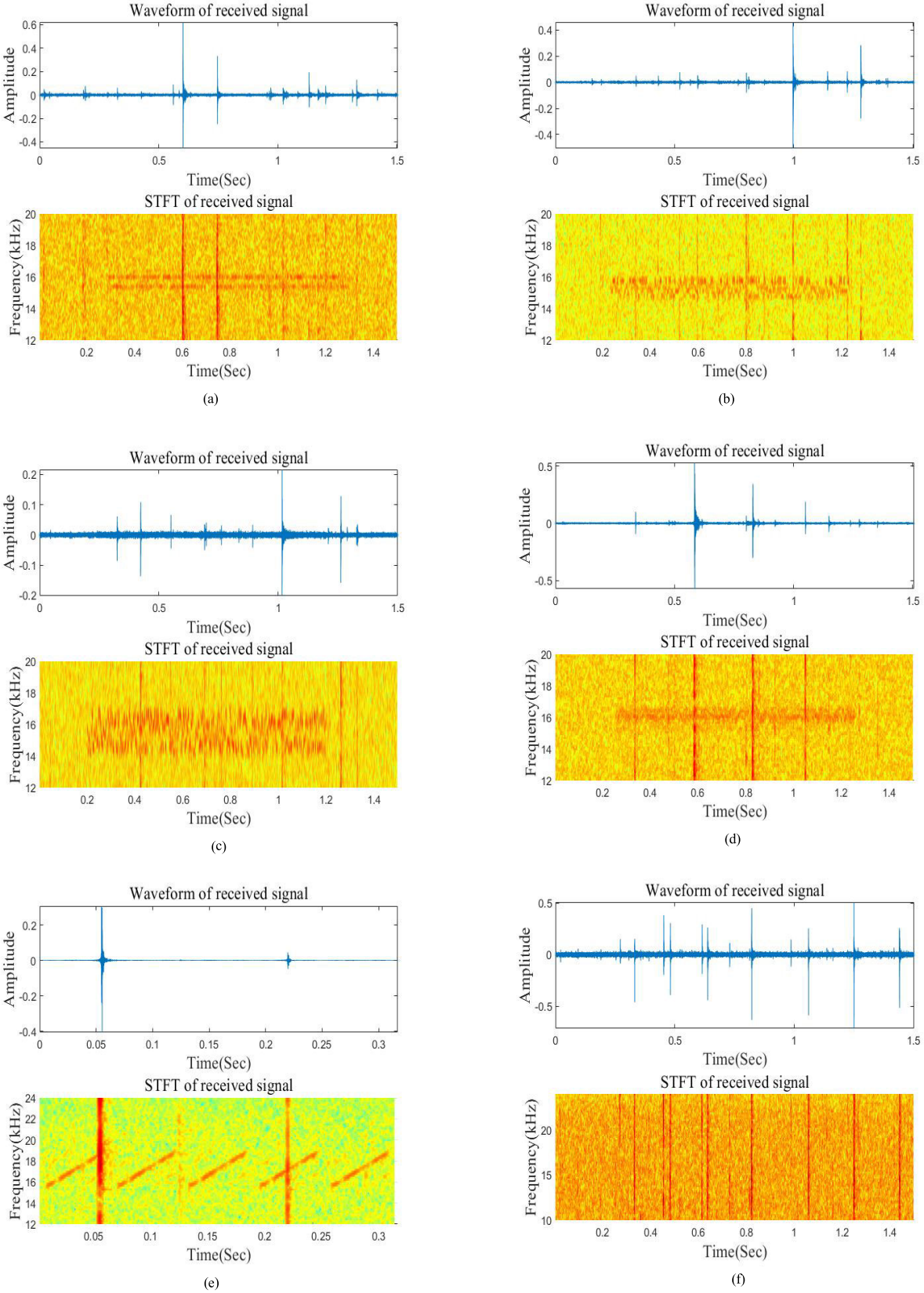

FIGURE 14. Temporal waveforms and STFT of different signal examples collected from the artificial lake: (a) 2FSK; (b) 4FSK; (c) 8FSK; (d) BPSK; (e) LFM; (f) Noise.

The testing set is formed along with 7000 more noise examples. Figs. 13 and 14 show the temporal waveforms and short-time Fourier transformation (STFT) of several signal examples collected from Wuyuan Bay and the artificial lake, respectively.

As shown in Fig. 13, the UWAC signals collected from Wuyuan Bay are contaminated with intense impulsive noise, and the SNR is low. The characteristic exponent α is estimated to be in the range of [1.16, 1.95] with the method of sample fractiles proposed in [46]. For the signals collected in the artificial lake, α is estimated to be in the range of [1.54, 2.0]. Fig. 15 shows the power spectrum images of the BPSK signal examples shown in Figs. 13(d) and 14(d). It is evident that the signal collected from the artificial lake has a lower SNR, and the corresponding ambient noise has a wider dynamic range.

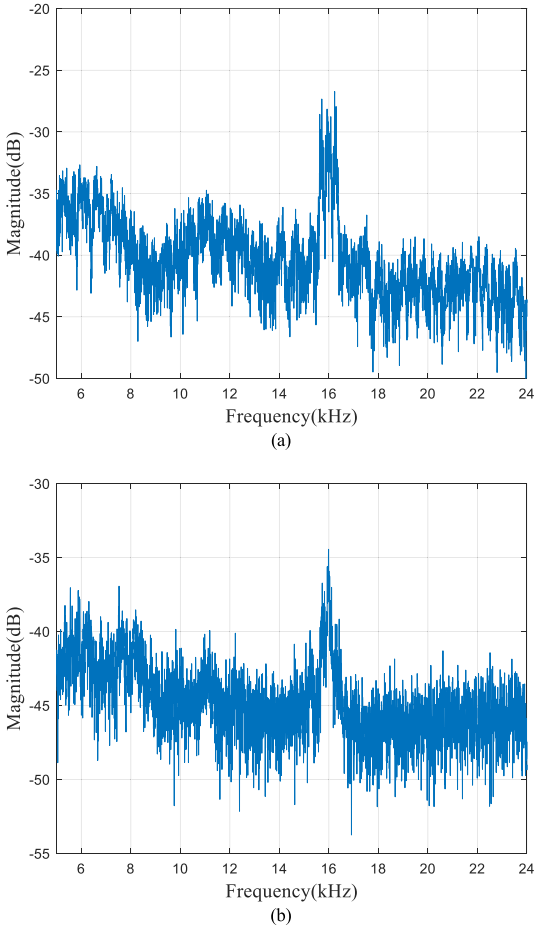

FIGURE 15. Power spectrum images of BPSK signal examples collected from: (a) Wuyuan Bay; (b) Artificial lake.

To prove the effectiveness of the proposed method, the detection performance is compared with that of the FLOMD and SLD methods. The fractional moment' order of the FLOMD is set to 0.3. The threshold parameter of the SLD is set to be the median of the absolute values of the observed signal samples. Fig. 16. shows the ROC curves of the two methods in the different water regions.

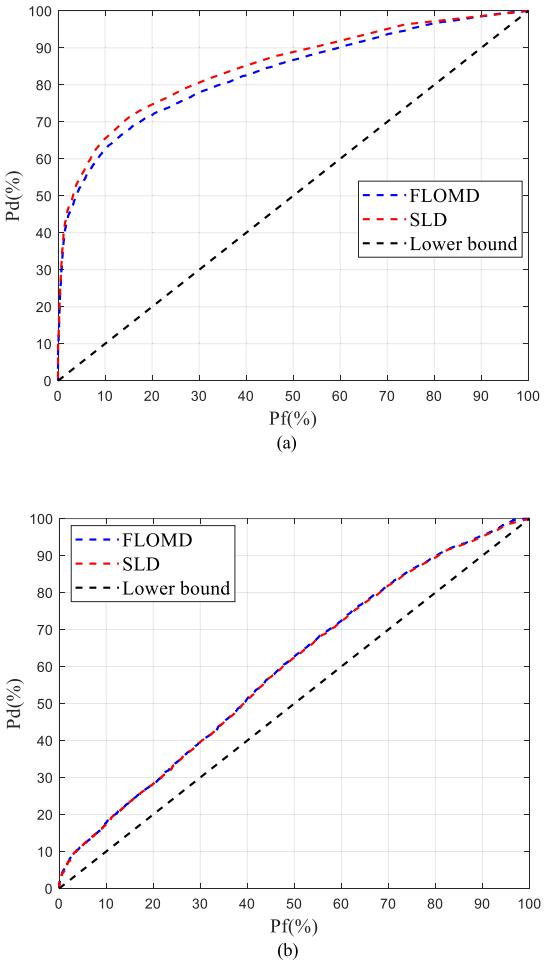

FIGURE 16. ROC curves of the FLOMD and SLD in different water regions: (a) Wuyuan Bay; (b) Artificial lake.

As shown in Fig. 16, the detection performance of the two methods in the artificial lake experiment is much worse than that in the Wuyuan Bay experiment. This result can be attribute to the lower SNR and wider dynamic range of noise, as shown in Fig. 15. Moreover, because no decision threshold is required for the proposed method, the Pf and Pd values are fixed given a certain testing set. Therefore, for the sake of comparison, we choose the Pd value when the same Pf value as in our approach is obtained for the FLOMD and SLD. Table 8 lists the detection results for the signals collected from Wuyuan Bay and the artificial lake.

As listed in Table 8, the proposed method has a high Pd value of 99.943% in the Wuyuan Bay experiment, whereas those of the FLOMD and SLD are only 60.44% and 63.15%, respectively. However, the Pf value reaches 8.357%, i.e., a small number of noise examples is misjudged as UWAC signals. Fig. 17 shows the temporal waveforms and STFT of two typical false-alarm noise examples.

TABLE 8. Detection performance on practical signals.

Methods	Wuyuan Bay (Pf = 8.357%)	Artificial lake (Pf = 0.286%)
Proposed method	99.943%	99.857%
FLOMD	60.44%	2.8%
SLD	63.15%	1.9%

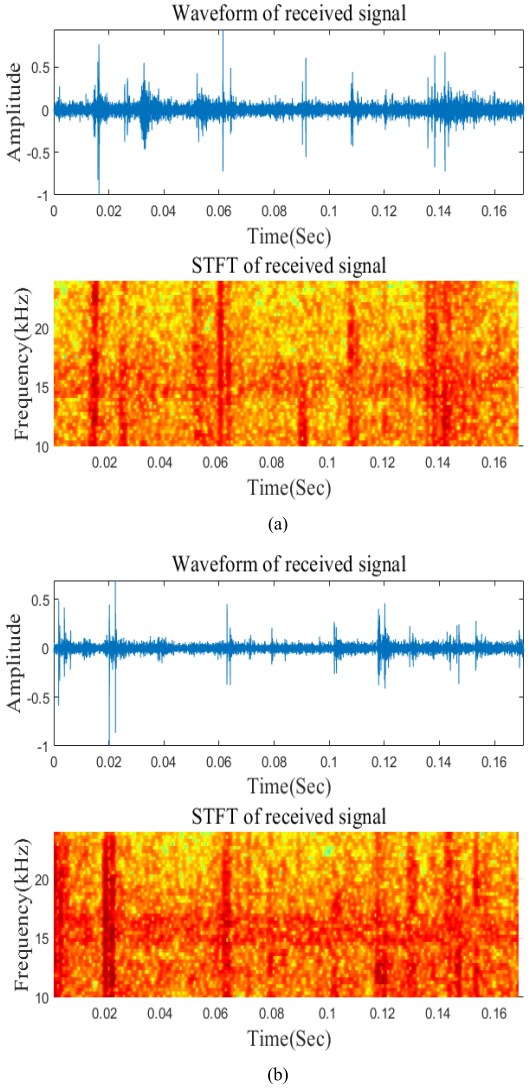

FIGURE 17. Temporal waveforms and STFT of two typical false-alarm noise examples: (a) Example one; (b) Example two.

As shown in Fig. 17, in addition to the heavy alpha-stable distributed noise, the two noise examples have another common aspect. The STFT images show that there are both intense interferences in the frequency range of approximately 14–17 kHz, which is within the communication frequency band (i.e., 13 to 18 kHz) of our dataset. Moreover, these interferences last almost the entire duration of the examples, which can be easily distinguished from Fig. 13(f). These characteristics make them similar to the noisy UWAC signal examples. Thus, the Pf value is increased.

When it comes to the artificial lake experiment, Table 8 shows that our method retains a high Pd value and a low Pf value of 99.857% and 0.286%, respectively. However, the detection performance of the two statistical detection theory-based methods decreases significantly, because of the low SNR and intense noise of a wider dynamic range. The Pd values of the FLOMD and SLD are 2.8% and 1.9%, respectively. The above results indicate that the proposed method is more effective and robust in practical underwater acoustic environments.

Furthermore, to prove that the proposed C can extract effective features for detection, the t-SNE technique [47] is adopted to visualize the output of the intermediate layer. Typically, the convolution layers of a CNN are considered feature extractors, and the deeper the layer, the more advanced the learned features. For the proposed C, the final convolution layer (i.e., Conv17) is designed for the compression of the feature channels. Thus, we selected the output of the penultimate convolution layer (i.e., Conv16), which is a vector of dimension 256×8. The learned features are then mapped to a 2D plane. Fig. 18 shows the visualization.

As shown in Fig. 18, the features extracted from the signals collected in Wuyuan Bay are mainly distributed in two clusters. The noise cluster has a relatively narrow distribution, whereas the signal cluster is made of several small clusters, because of category diversity. Moreover, a small number of noise features is mistakenly distributed in the signal cluster, which well corresponds with the results listed in Table 8.

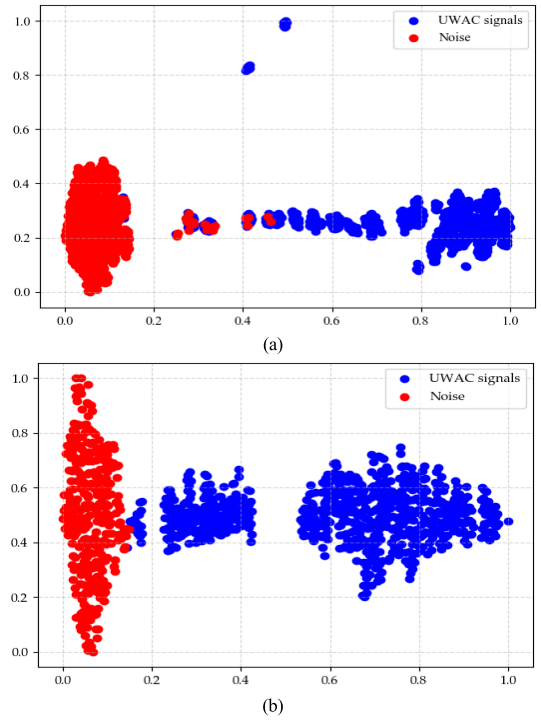

FIGURE 18. T-SNE plot for the detection features of practical signals collected from: (a) Wuyuan Bay; (b) Artificial lake.

When it comes to the artificial lake experiment, the margin of the two clusters is more evident, and fewer features are incorrectly distributed. These results demonstrate that the proposed C can steadily extract the essential features of the denoised signals for detection.

IV. CONCLUSION

In this study, we developed a blind detection method for UWAC signals based on DL. First, an INP and SDGAN were built to mitigate the noise in the received signals. The denoised signals were then fed to a CNN-based classifier for feature extraction and binary classification. Moreover, a transfer data model was proposed to address the data scarcity problem. The results of simulation experiments and practical signal tests both demonstrated that the proposed method is robust against ambient noise with wide dynamic ranges and complex distributions. Moreover, our approach significantly outperformed existing methods under low-SNR conditions, while requiring no prior information about the testing channel.

In the future, we intend to extend this method to the detection of other underwater acoustic signals and improve the existing blind detection algorithms for RS signals under complex environments.

REFERENCES

[1] Q. Li, M. Li, and X. Yang, "The detection of single frequency component of underwater radiated noise of target: Theoretical analysis," *Acta Acust.*, vol. 33, no. 3, pp. 193–196, May 2008.

[2] Y. Li and Z. Chen, "Entropy based underwater acoustic signal detection," in *Proc. 14th Int. Bhurban Conf. Appl. Sci. Technol. (IBCAST)*, Jan. 2017, pp. 656–660.

[3] T. Yi, X. Xiaomei, and Z. Minghui, "Application of stochastic resonance theory in weak underwater acoustic signal detection," in *Proc. IEEE 12th Int. Conf. Commun. Technol.*, Nov. 2010, pp. 1268–1270.

[4] J. Liu, X.-K. Li, T. Ma, S.-C. Piao, and Q.-Y. Ren, "An improved Hilbert-huang transform and its application in underwater acoustic signal detection," in *Proc. 2nd Int. Congr. Image Signal Process.*, Oct. 2009, pp. 1–5.

[5] C. R. Baker, A. Climescu-Haulica, and A. F. Gualtierotti, "Likelihood ratio methods for underwater acoustics signal detection," in *Proc. 5th IMA Conf. Math. Signal Process.*, Dec. 2000, pp. 1–13.

[6] G. A. Tsihrintzis and C. L. Nikias, "Performance of optimum and suboptimum receivers in the presence of impulsive noise modeled as an alpha-stable process," *IEEE Trans. Commun.*, vol. 43, nos. 2–4, pp. 904–914, Feb. 1995.

[7] J. G. Gonzalez and G. R. Arce, "Optimality of the myriad filter in practical impulsive-noise environments," *IEEE Trans. Signal Process.*, vol. 49, no. 2, pp. 438–441, Feb. 2001.

[8] X. Zhu, W.-P. Zhu, and B. Champagne, "Spectrum sensing based on fractional lower order moments for cognitive radios in α-stable distributed noise," *Signal Process.*, vol. 111, pp. 94–105, Jun. 2015.

[9] L. Junshan, W. Shilian, and Z. Wei, "Fractile-piecewise processing based spectrum sensing algorithms for underwater cognitive acoustics with impulsive noise," in *Proc. 11th ACM Int. Conf. Underwater Netw. Syst. - WUWNet*, 2016, pp. 1–2.

[10] T. C. Yang and W.-B. Yang, "Low probability of detection underwater acoustic communications using direct-sequence spread spectrum," *J. Acoust. Soc. Amer.*, vol. 124, no. 6, pp. 3632–3647, Dec. 2008.

[11] J. Luo, S. Wang, W. Zhang, and Q. Cheng, "Fractional lower-order autocorrelation detection of underwater direct sequence spread spectrum signals in impulsive noise," in *Proc. OCEANS MTS/IEEE Kobe Techno-Oceans (OTO)*, May 2018, pp. 1–4.

[12] H. Oh and H. Nam, "Energy detection scheme in the presence of burst signals," *IEEE Signal Process. Lett.*, vol. 26, no. 4, pp. 582–586, Apr. 2019.

[13] K. Ruttik, K. Koufos, and R. Jantti, "Detection of unknown signals in a fading environment," *IEEE Commun. Lett.*, vol. 13, no. 7, pp. 498–500, Jul. 2009.

[14] G. Chu, K. Niu, W. Wu, F. Yang, and W. Jiang, "Performance evaluation of spectrum sensing based on wavelet entropy for cognitive radio networks," in *Proc. Int. Symp. Wireless Pers. Multimedia Commun. (WPMC)*, Sep. 2014, pp. 434–438.

[15] K. M. Hock, "Narrowband weak signal detection by higher order spectrum," *IEEE Trans. Signal Process.*, vol. 44, no. 4, pp. 874–879, Apr. 1996.

[16] T. Cheng, C. Liu, and W. Ding, "Weak signal detection based on deep learning," in *Proc. 4th Int. Conf. Multimedia Syst. Signal Process. ICMSSP*, May 2019, pp. 114–118.

[17] D. Ke, Z. Huang, X. Wang, and X. Li, "Blind detection techniques for non-cooperative communication signals based on deep learning," *IEEE Access*, vol. 7, pp. 89218–89225, 2019.

[18] J. Gao, X. Yi, C. Zhong, X. Chen, and Z. Zhang, "Deep learning for spectrum sensing," *IEEE Wireless Commun. Lett.*, vol. 8, no. 6, pp. 1727–1730, Dec. 2019.

[19] X. Zha, H. Peng, X. Qin, G. Li, and S. Yang, "A deep learning framework for signal detection and modulation classification," *Sensors*, vol. 19, no. 18, p. 4042, Sep. 2019.

[20] H. Wang, O. A. Dobre, C. Li, and D. C. Popescu, "Blind cyclostationarity-based symbol period estimation for FSK signals," *IEEE Commun. Lett.*, vol. 19, no. 7, pp. 1149–1152, Jul. 2015.

[21] A. Punchihewa, O. A. Dobre, S. Rajan, and R. Inkol, "Cyclostationarity-based algorithm for blind recognition of OFDM and single carrier linear digital modulations," in *Proc. IEEE 18th Int. Symp. Pers., Indoor Mobile Radio Commun.*, Dec. 2007, pp. 1–5.

[22] J. Yu, L. Zhang, and K. Liu, "Coherently distributed wideband LFM source localization," *IEEE Signal Process. Lett.*, vol. 22, no. 4, pp. 504–508, Apr. 2015.

[23] S. G. Gilsic, Z. B. Nikolic, D. Pokrajac, and P. A. Leppanen, "Performance enhancement of DSSS systems: Two-dimensional interference suppression," *IEEE Trans. Commun.*, vol. 47, no. 10, pp. 1549–1560, Oct. 1999.

[24] J. G. Veitch and A. R. Wilks, "A characterization of arctic undersea noise," *J. Acoust. Soc. Amer.*, vol. 77, no. 3, pp. 989–999, Mar. 1985.

[25] M. Chitre, J. Potter, and O. Sim Heng, "Underwater acoustic channel characterisation for medium-range shallow water communications," in *Proc. Oceans MTS/IEEE Techno-Ocean*, Mar. 2004, pp. 40–45.

[26] B. Hu and D. Yang, "Symmetic alpha-stable distributions for analysis of underwater impulsive noise," *Tech. Acoust.*, vol. 25, no. 2, pp. 134–139, Apr. 2006.

[27] G. Samorodnitsky and M. S. Taqqu, "Stable non-Gaussian random processes: Stochastic models with infinite variance," *J. Amer. Stat. Assoc.*, vol. 90, no. 430, pp. 805–806, 1995.

[28] T. Qiu, X. Zhang, X. Li, and Y. Sun, *Statistical Signal Processing: Non Gaussian Signal Processing and its Application*. Beijing, China: China Water Power Press, 2004, pp. 184–186.

[29] R. Barazideh, W. Sun, B. Natarajan, A. V. Nikitin, and Z. Wang, "Impulsive noise mitigation in underwater acoustic communication systems: Experimental studies," in *Proc. IEEE 9th Annu. Comput. Commun. Workshop Conf. (CCWC)*, Jan. 2019, pp. 880–885.

[30] V. Nuthna, K. Chachadi, and L. S. Joshi, "Modeling and performance evaluation of generative adversarial network for image denoising," in *Proc. Int. Conf. Comput. Techn., Electron. Mech. Syst. (CTEMS)*, Dec. 2018, pp. 7–11.

[31] S. Pascual, A. Bonafonte, and J. Serrà, "SEGAN: Speech enhancement generative adversarial network," in *Proc. Interspeech*, Aug. 2017, pp. 3642–3646.

[32] D. Baby and S. Verhulst, "Sergan: Speech enhancement using relativistic generative adversarial networks with gradient penalty," in *Proc. ICASSP - IEEE Int. Conf. Acoust., Speech Signal Process. (ICASSP)*, May 2019, pp. 106–110.

[33] I. J. Goodfellow, J. Pouget-Abadie, M. Mirza, B. Xu, D. Warde-Farley, S. Ozair, A. Courville, and Y. Bengio, "Generative adversarial networks," in *Proc. Adv. Neural Inf. Process. Syst.*, vol. 3, 2014, pp. 2672–2680.

[34] P. Vincent, H. Larochelle, Y. Bengio, and P.-A. Manzagol, "Extracting and composing robust features with denoising autoencoders," in *Proc. 25th Int. Conf. Mach. Learn. - ICML*, 2008, pp. 1096–1103.

[35] K. He, X. Zhang, S. Ren, and J. Sun, "Deep residual learning for image recognition," in *Proc. IEEE Conf. Comput. Vis. Pattern Recognit. (CVPR)*, Jun. 2016, pp. 770–778.

[36] J. Li, J. Jia, and D. Xu, "Unsupervised representation learning of image-based plant disease with deep convolutional generative adversarial networks," in *Proc. 37th Chin. Control Conf. (CCC)*, Jul. 2018, pp. 1–6.
[37] K. He, X. Zhang, S. Ren, and J. Sun, "Delving deep into rectifiers: Surpassing human-level performance on ImageNet classification," in *Proc. IEEE Int. Conf. Comput. Vis. (ICCV)*, Dec. 2015, pp. 1026–1034.
[38] M. Arjovsky and L. Bottou, "Towards principled methods for training generative adversarial networks," in *Proc. Int. Conf. Learn. Represent. (ICLR)*, Apr. 2017, pp. 1–17.
[39] X. Mao, Q. Li, H. Xie, R. Y. K. Lau, Z. Wang, and S. P. Smolley, "Least squares generative adversarial networks," in *Proc. IEEE Int. Conf. Comput. Vis. (ICCV)*, Oct. 2017, pp. 2813–2821.
[40] M. Arjovsky, S. Chintala, and L. Bottou, "Wasserstein generative adversarial network," in *Proc. Int. Conf. Mach. Learn. (ICML)*, Aug. 2017, pp. 214–223.
[41] I. Gulrajani, F. Ahmed, M. Arjovsky, V. Dumoulin, and A. Courville, "Improved training of Wasserstein GANs," in *Proc. 31st Int. Conf. Neural Inf. Process. Syst. (NIPS)*, Mar. 2017, pp. 5769–5779.
[42] A. Jolicoeur-Martineau, "The relativistic discriminator: A key element missing from standard GAN," in *Proc. Int. Conf. Learn. Represent. (ICLR)*, May 2019, pp. 1–26.
[43] D. P. Kingma and J. L. Ba, "Adam: A method for stochastic optimization," in *Proc. Int. Conf. Learn. Represent. (ICLR)*, May 2015, pp. 1–15.
[44] X. Ning, Z. Liu, Y. Luo, and C. Sun, "Fast convergence adaptive equalization algorithm for underwater acoustic channels," *Syst. Eng. Electron.*, vol. 32, no. 12, pp. 2524–2527, Dec. 2010.
[45] S. Zhou and X. Zeng, "A de-noising method for underwater acoustic signals based on CEEMDAN," *Tech. Acoust.*, vol. 36, no. 5, pp. 263–264, Oct. 2017.
[46] J. H. McCulloch, "Simple consistent estimators of stable distribution parameters," *Commun. Statist. Simul. Comput.*, vol. 15, no. 4, pp. 1109–1136, 1986.
[47] A. Karpathy, J. Johnson, and L. Fei-Fei, "Visualizing and understanding recurrent networks," 2015, *arXiv:1506.02078*. [Online]. Available: http://arxiv.org/abs/1506.02078

YONGBIN LI was born in 1996. He received the B.S. degree from Information Engineering University, in 2018, where he is currently pursuing the master's degree. His research interest includes underwater acoustic communication signal processing.

BIN WANG received the Ph.D. degree from Information Engineering University, in 2007. Her research interest includes underwater acoustic communication signal processing.

GAOPING SHAO received the Ph.D. degree from the Beijing Institute of Technology, in 2009. His research interest includes communication signal processing.

SHUAI SHAO received the M.S. degree from the University of Central Lancashire, in 2014. His research interests include digital signal and image processing.

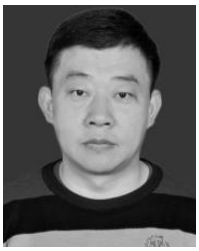

XILONG PEI received the M.S. degree from Information Engineering University, in 2006. His research interest includes communication signal processing.